Published in the Proceedings of
2012 IEEE Computer Society Workshop on Mathematical Methods in
Biomedical Image Analysis (MMBIA). pp 25-32.

Sparse Shape Representation using the Laplace-Beltrami Eigenfunctions and Its Application to Modeling Subcortical Structures

Seung-Goo Kim[1] sol@snu.ac.kr
Moo K. Chung[1,2,3*] mkchung@wisc.edu
Stacey M. Schaefer[2] smschaefer2@wisc.edu
Carien van Reekum[5] c.vanreekum@reading.ac.uk
Richard J. Davidson[2,4] rjdavids@wisc.edu

[1]Department of Brain and Cognitive Sciences, Seoul National University, Korea
[2]Waisman Laboratory for Brain Imaging and Behavior,
[3]Department of Biostatistics and Medical Informatics,
[4]Department of Psychology and Psychiatry, University of Wisconsin, Madison, WI, USA.
[5]Centre for Integrative Neuroscience and Neurodynamics,
School of Psychology and Clinical Language Sciences, University of Reading, UK.

Abstract

We present a new sparse shape modeling framework on the Laplace-Beltrami (LB) eigenfunctions. Traditionally, the LB-eigenfunctions are used as a basis for intrinsically representing surface shapes by forming a Fourier series expansion. To reduce high frequency noise, only the first few terms are used in the expansion and higher frequency terms are simply thrown away. However, some lower frequency terms may not necessarily contribute significantly in reconstructing the surfaces. Motivated by this idea, we propose to filter out only the significant eigenfunctions by imposing l_1-penalty. The new sparse framework can further avoid additional surface-based smoothing often used in the field. The proposed approach is applied in investigating the influence of age (38-79 years) and gender on amygdala and hippocampus shapes in the normal population. In addition, we show how the emotional response is related to the anatomy of the subcortical structures.

*Corresponding address: Moo K. Chung, Waisman Center #281, 1500 Highland Ave. Madison, WI., 53705. telephone: 608-217-2452, http://www.stat.wisc.edu/~mchung/.

1. Introduction

The general tendency of atrophy of brain tissues associated with the increase of age is extensively examined by postmortem studies [19] and *in-vivo* studies using magnetic resonance imaging (MRI) of several hundreds subjects [11, 34]. However, the age effect on subcortical structures has been somewhat controversial [30, 34]. The adverse effect of aging on amygdalar and hippocampal structures has drawn much attention [5, 9, 11, 23, 29, 30, 33, 34]. While many cross sectional [5, 9, 33] and longitudinal [23] studies reported significant reduction in regional volume of amygdala and hippocampus due to aging, others failed to confirm such relationship [11, 29, 30, 34]. Gender may be another factor that affects these structures. One study reported significant gender effect in amygdala and hippocampus volume [10] whereas others failed to replicate the finding [12].

In these previous volumetric studies, the total volume of the amygdala and hippocampus were typically estimated by tracing the region of interest (ROI) manually and counting the number of voxels within the ROI. The limitation of the ROI-based volumetry is that it cannot determine if the volume difference is diffuse over the whole ROI or localized within specific regions of the ROI [7]. The proposed sparse shape representation can localize the volume difference up to the mesh resolution at each surface mesh vertex.

Starting with the 3D deformation field derived from the

spatial normalization of MRI, we can model how the surfaces of subcortical structures are different from each other at the vertex level. Since the deformation field is noisy, it is necessary to smooth out the field along the surface to increase the signal-to-noise ratio (SNR). Further, smoothing is desirable in satisfying the assumptions of the random field theory (RFT), which is used in correcting for multiple comparisons [1, 36]. For RFT to work, the Gaussianness and smoothness of data are needed [1, 35]. With this motivation, we present a new framework that sparsely filter out significant coefficients in the LB-eigenfunction expansion using the l_1-norm penalty, which is often used in compressed sensing and sparse regression. The proposed framework is then used in examining the effect of age and gender on amygdala and hippocampus shapes, contrasting the traditional volumetric analysis. We further show how to model the emotional response on the subcortical structure shapes.

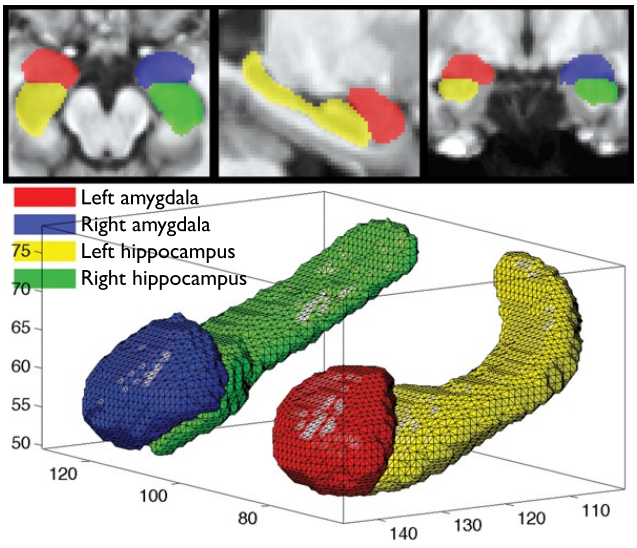

Figure 1: Binary masks for subcortical structures (top) and the surfaces of the binary masks (bottom).

2. Method

The proposed pipeline for sparse shape modeling is as follows: (1) obtain a mean volume of a subcortical structure by averaging the spatially normalized binary masks, and extract a template surface from the averaged binary volume, (2) interpolate the 3D displacement vector field onto the vertices of the surface meshes, (3) estimate a sparse representation of Fourier coefficients with l_1-norm penalty for the displacement length along the template surface to reduce noise, and (4) apply a general linear model (GLM) testing the effect of age and gender on the displacement. The interaction between age and emotional response is also tested. The detailed description of each step is given in section 2 and the statistical inference results are given in section 3.

2.1. Images and preprocessing

We have high-resolution T1-weighted inverse recovery fast gradient echo MRI, collected in 124 contiguous 1.2-mm axial slices (TE=1.8 ms; TR=8.9 ms; flip angle = 10°; FOV = 240 mm; 256 × 256 data acquisition matrix) of 52 middle-age and elderly adults ranging between 37 to 74 years (mean age = 55.52 ± 10.40 years). There are 16 men and 36 women in the study. Trained raters manually segmented the amygdala and hippocampus structures. Brain tissues in the MRI scans were automatically segmented using Brain Extraction Tool (BET) [26]. Then we performed a nonlinear image registration using the diffeomorphic shape and intensity averaging technique with the cross-correlation as the similarity metric through Advanced Normalization Tools (ANTS) [4]. A study-specific template was constructed from a random subsample of 10 subjects.

Using the deformation field obtained from warping the individual image to the template, we aligned the amygdala and hippocampus binary masks to the template space. The normalized masks were then averaged to produce the subcortical structure template. The isosurfaces of the subcortical structure template were extracted using the marching cube algorithm [17]. The masked volumes for the subcortical structures and the corresponding isosurfaces are shown in Fig. 1.

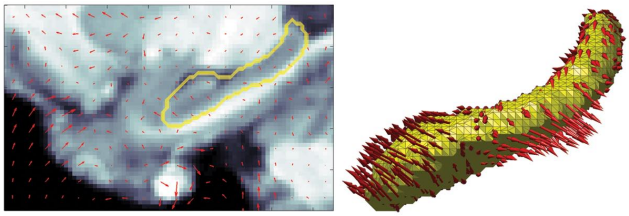

Figure 2: The displacement vector field (red arrows) on the sagittal slice of the template (left). The outline of the left hippocampus is drawn in yellow. The displacement vector field on the mesh vertices is interpolated from the voxels (right).

The displacement vector field is defined on each voxel, while the vertices of mesh are located within a voxel. So we linearly interpolated the vector field on mesh vertices from the voxels (Fig. 2). The length of the displacement vector at each vertex is computed and used as a feature to measure the local shape variation with respect to the template space.

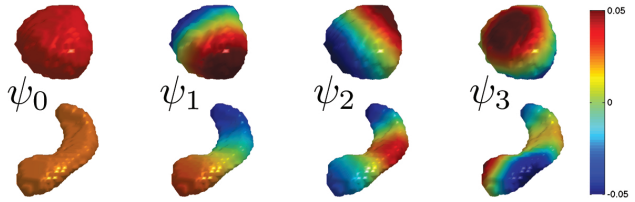

Figure 3: Examples of the Laplace-Beltrami eigenfunctions of the left amygdala (top) and the left hippocampus (bottom): first four eigenfunctions $\psi_0, \psi_1, \psi_2, \psi_3$ are shown.

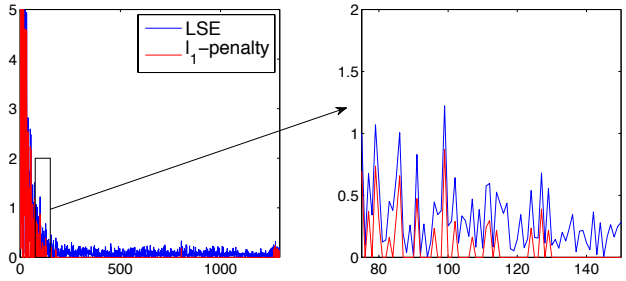

Figure 4: Absolute values of Fourier coefficients obtained using the LSE (blue) and the l_1-penalty (red) for the length of displacement of a subject on the left amygdala.

2.2. Sparse representation using an l_1-penalty

Since the lengths of displacement defined on mesh vertices are expected to be noisy due to errors associated with image acquisition and image preprocessing, it is necessary to smooth out the noise and increase the signal-to-noise ratio [7]. Many previous surface data smoothing approaches have used heat diffusion type of smoothing to reduce surface noise [3, 7, 18, 20, 27, 31, 32].

Instead, we propose to use the Laplace-Beltrami (LB) eigenfunctions in parametrically representing the surface data. In previous LB-eigenfunction and similar spherical harmonic (SPHARM) expansion approaches only the first few terms are used in the expansion and higher frequency terms are simply thrown away [21, 24, 28] to reduce the high frequency noise. However, some lower frequency terms may not necessarily contribute significantly in reconstructing the surfaces. Motivated by this idea, we propose to sparsely filter out insignificant eigenfunctions by imposing the l_1-penalty [13].

Consider a real-valued functional measurement $Y(p)$ on a manifold $\mathcal{M} \subset \mathbb{R}^3$. We assume the following additive model:

$$Y(p) = \theta(p) + \epsilon(p), \tag{1}$$

where $\theta(p)$ is the unknown mean signal to be estimated and $\epsilon(p)$ is a zero-mean Gaussian random field.

Solving

$$\Delta\psi_j = \lambda_j\psi_j, \tag{2}$$

on $\mathcal{M}$, we find the eigenvalues λ_j and eigenfunctions ψ_j. The eigenfunctions ψ_j form an orthonormal basis in $L^2(\mathcal{M})$, the space of square integrable functions on $\mathcal{M}$ [16]. We may order eigenvalues as

$$0 = \lambda_0 < \lambda_1 \leq \lambda_2 \cdots$$

and corresponding eigenfunctions as $\psi_0, \psi_1, \psi_2, \cdots$.

Since the closed form expression for the eigenfunctions of the LB-operator on an arbitrary curved surface is unknown, the eigenfunctions are numerically estimated by discretizing the LB-operator. Using the Cotan discretization [6, 21], (2) is linearized as the generalized eigenvalue problem:

$$\mathbf{C}\boldsymbol{\psi} = \lambda\mathbf{A}\boldsymbol{\psi}, \tag{3}$$

where $\mathbf{C}$ is the stiffness matrix, $\mathbf{A}$ is the mass matrix and $\boldsymbol{\psi} = (\psi(p_1), \cdots, \psi(p_n))'$ is the unknown eigenfunction evaluated at n mesh vertices [24]. The first few eigenfunctions for the subcortical surfaces are shown in Fig. 3.

Once we obtained the eigenfunctions ψ_j, we can parametrically estimate the unknown mean signal $\theta(p)$ as the Fourier expansion as

$$\theta(p) = \sum_{i=0}^{k} \beta_j\psi_j,$$

where β_j is the Fourier coefficients to be estimated. The truncation degree k is usually low. In Styer et al., 12 and 15 degree SPHARM expansions were used for hippocampus and caudate respectively [28]. The Fourier coefficients can be obtained by the usual least squares estimation (LSE) by solving

$$\mathbf{Y} = \boldsymbol{\psi}\boldsymbol{\beta}, \tag{4}$$

where $\mathbf{Y} = (Y(p_1), \cdots, Y(p_n))'$, $\boldsymbol{\beta} = (\beta_1, \cdots, \beta_k)'$ and $\boldsymbol{\psi} = (\psi_i(p_j))$ is an $n \times k$ matrix of eigenfunctions evaluated at mesh vertices [39]. The LSE is then given as

$$\widehat{\boldsymbol{\beta}} = (\boldsymbol{\psi}'\boldsymbol{\psi})^{-1}\boldsymbol{\psi}'\mathbf{Y}. \tag{5}$$

The estimation, however, may include low degree coefficients that do not contribute significantly. Therefore, instead of using LSE, we introduce the additional l_1-norm penalty to sparsely filter out insignificant low degree coefficients by minimizing [13]:

$$\|\mathbf{Y} - \boldsymbol{\psi}\beta\|_2^2 + \lambda\|\beta\|_1, \tag{6}$$

where the parameter $\lambda > 0$ controls the amount of sparsity. We have used $\lambda = 1$ for our study. This results in 72.87

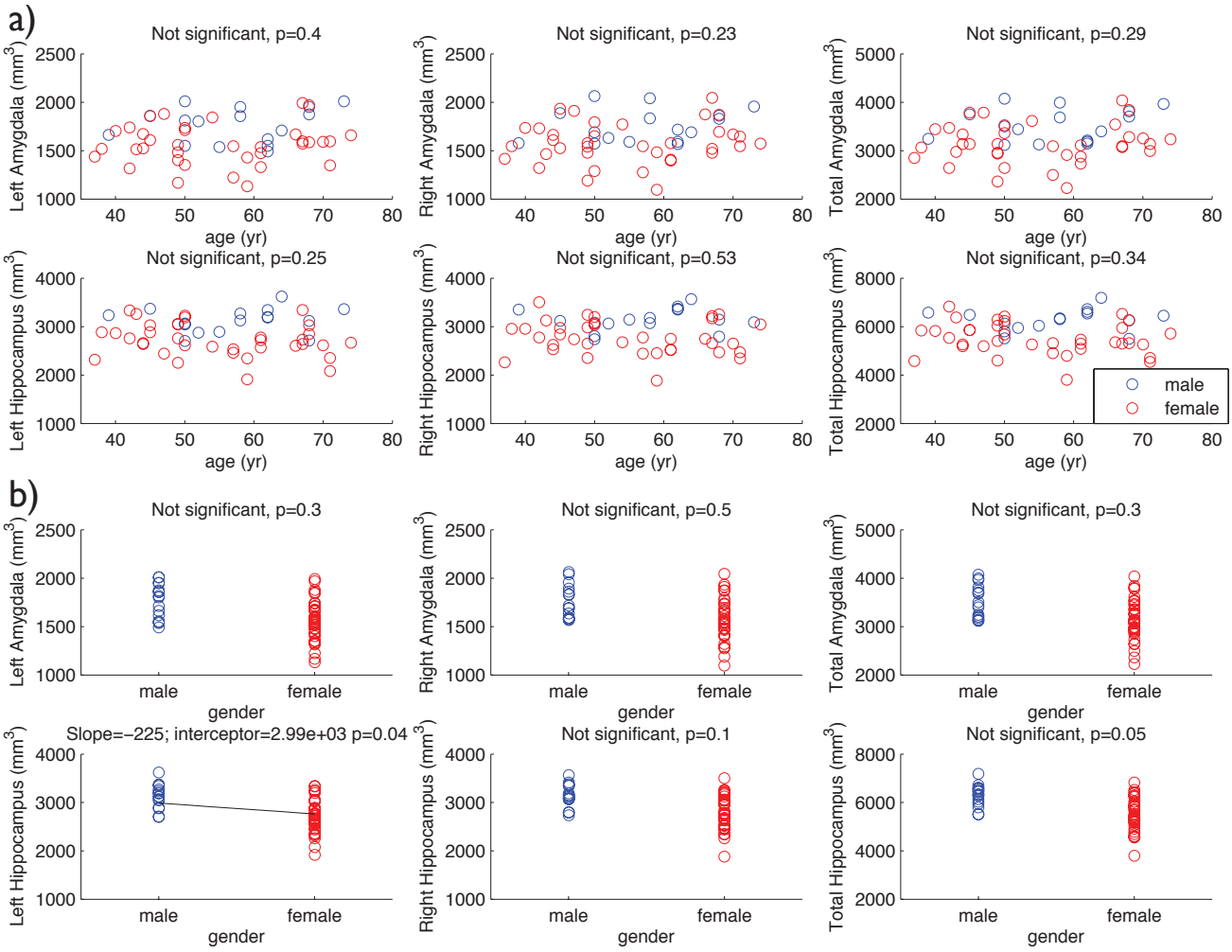

Figure 5: Scatterplots of amygdala and hippocampus volumes over age (a) and gender (b).

non-zero coefficients out of 1310 in average for amygdale (5.56%) and 133.09 non-zero coefficients out of 2499 in average for hippocampi (5.33%). As an illustration, the absolute values of coefficients estimated by LSE and l_1-penalty with the first 1295 eigenfunctions for the length of displacement of a subject on the left amygdala are shown in Figure 4.

3. Results

We have applied our sparse shape modeling framework in determining the effects of age, gender and behavioral response on the shape of amygdala and hippocampus. We demonstrate that the proposed l_1-penalty approach can detect the localized effects within the cortical substructures while the traditional method cannot.

3.1. Traditional volumetric analysis

In the traditional approach, the volume of a structure is simply computed by counting the number of voxels within the binary mask. In order to account for the effect of inter-subject variability in brain size, the brain volume except cerebellum was estimated and covariated in general linear models (GLM).

The brain volume is significantly correlated with the amygdala (left: $p < 10^{-4}$; right: $p < 10^{-4}$) and the hippocampus volumes (left: $p < 10^{-5}$; right: $p < 10^{-6}$). Here p indicates the p-values. Since amygdala and hippocampus volumes are dependent on the whole brain volume, we need to factor out the brain volume in the subsequent statistical analysis.

We model the Volume of amygdala and hippocampus

as

$$\mathrm{Volume} = \beta_1 + \beta_2 \cdot \mathrm{Brain} + \beta_3 \cdot \mathrm{Age} + \beta_4 \cdot \mathrm{Gender} + \epsilon, \quad (7)$$

where ϵ is zero mean Gaussian noise and Brain is the total brain volume. The age and gender effects were determined by testing the significance of parameters β_3 and β_4 at $\alpha = 0.05$. The results are displayed in Figure 5.

We did not find a significant age effect on the amygdala (left $p = 0.40$; right $p = 0.23$; combined $p = 0.29$) nor the hippocampus (left $p = 0.25$; right $p = 0.53$; combined $p = 0.34$). We only found a significant gender effect on the left hippocampus ($p = 0.04$), but no others (left amygdala $p = 0.26$; right amygdala $p = 0.47$; amygdalae combined $p = 0.34$; right hippocampus $p = 0.12$; hippocampi combined $p = 0.05$). Since the results are based on the whole volume of the amygdala and hippocampus, it is still unclear if there are any localized shape differences within the parts of the subcortical structures.

3.2. Subcortical structure shape analysis

The length of displacement vector field along the template surface was estimated using the sparse framework given in section 2. Then Length is regressed over the total brain volume and other variables:

$$\mathrm{Length} = \beta_1 + \beta_2 \cdot \mathrm{Brain} + \beta_3 \cdot \mathrm{Age} + \beta_4 \cdot \mathrm{Gender} + \epsilon. \quad (8)$$

The age and gender effects were determined by testing the significance of parameters β_3 and β_4 at $\alpha = 0.05$. We used SurfStat MATLAB toolbox for the statistical analysis and the multiple comparison correction based on the random field theory [7]. The results are displayed in Figure 6.

Age effect We found the region of significant effect of age on the posterior part of hippocampi (left: max $F = 33.48, p < 0.0002$; right: max $F = 18.48, p = 0.016$). Particularly, on the caudal regions of the left and right hippocampi, we found highly localized signals. It is consistent with other shape modeling studies on hippocampus [22, 37]. We did not find any age effects on the amygdala surface at $\alpha = 0.05$.

Gender effect We found the localize regions of gender effect on the amygdalae (left max $F = 16.90, p = 0.02$; right max $F = 26.41, p < 0.001$) and the left hippocampus (max $F = 25.35, p < 0.002$). In particular, the gender effects are found over the ventral part of laterobasal group of the right amygdala [2] and the anterior region of the CA1 subfield of the left hippocampus [38].

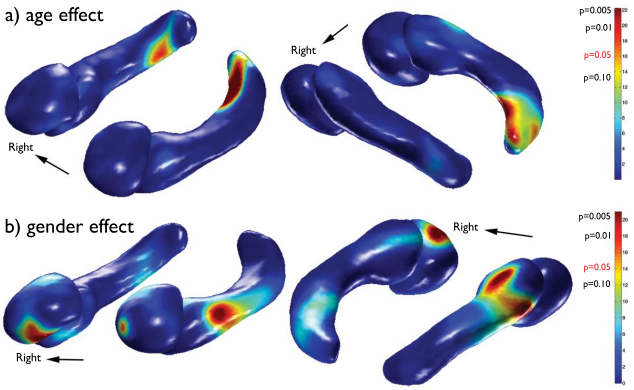

Figure 6: F-statistic maps on the amygdala and hippocampus surfaces showing the age (a) and gender (b) effects with the corresponding p-values.

The effect of proposed l_1-penalty framework is compared to that of LSE in Figure 7. Basically, the l_1-penalty regression approach penalizes insignificant low degree LB-coefficients while the LSE still retains them. In this study, only about 5% non-zero Fourier coefficients from LSE were used to reconstruct the surface in l_1-penalty. As a result, the l_1-penalty regression smooth out the resulting statistical map whereas LSE does not. Therefore, in order to apply RFT, the LSE-method still requires an additional surface-based data smoothing unlike l_1-penalty.

3.3. Effect of behavioral measure on anatomy

In addition, we further examined the effect of autonomic emotional response to the shape of the subcortical structures. Pictures from the international affective picture system (IAPS) [15], which cause negative, neutral or positive emotional responses, were presented to subjects with a 4-sec presentation time for each picture. While the subjects were seeing the pictures, an eye blink reflex (EBR) was induced by an auditory probe (105 dB SPL white noise for 50 ms) randomly at the one of the three predetermined timings (2.9, 4.4 and 5.9 sec after picture onset). 9 trials were made for each picture condition and timing, resulting $9\times3\times3$=81 trials in total. EBRs were recorded using electromyography (EMG). The magnitude of EBR was computed by subtracting the baseline EMG signal at the reflex onset from the maximal EMG signal between 20-120 ms after probe onset. Then the magnitude of EBR was standardized as a z-score within each subject to account for intersubject variability.

Once again, Length is regressed over the interaction of the age and EMG with other variables:

$$\begin{aligned}\mathrm{Length} = \beta_1 + \beta_2 \cdot \mathrm{Brain} + \beta_3 \cdot \mathrm{Age} + \beta_4 \cdot \mathrm{Gender} \\ + \beta_5 \cdot \mathrm{EMG} + \beta_6 \cdot \mathrm{Age} \cdot \mathrm{EMG} + \epsilon.\end{aligned} \quad (9)$$

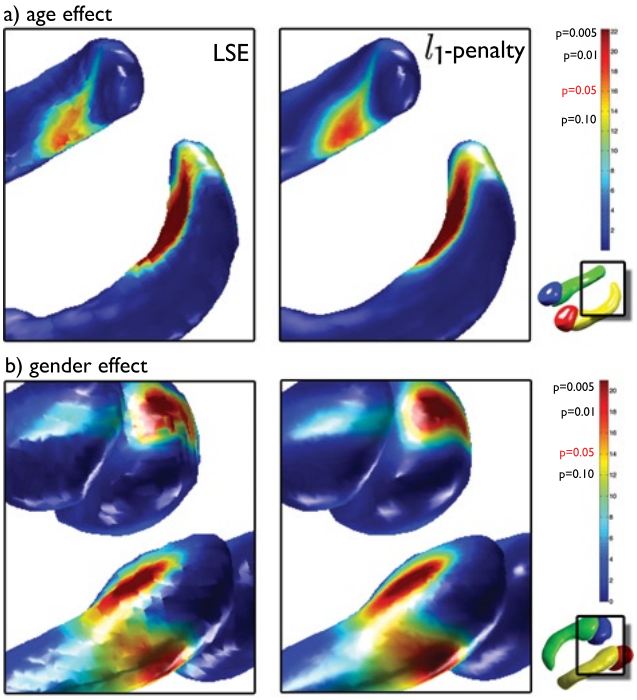

Figure 7: Comparison between the LSE (left) and the sparse regression (right) on F-statistic maps. Age (a) and gender (b) effects are shown respectively. The boxes over the small surface models under color-bars indicate the magnified areas in the panels (red: left amygdala, blue: right amygdala, yellow: left hippocampus, green: right hippocampus).

The EMG effect and the interaction between the age and the EMG were determined by testing the significance of parameters β_5 and β_6 at $\alpha = 0.05$. We have not found any significant EBR effects on subcortical regions among the EMG scores from 9 different types of trials (3 picture-conditions times 3 probe-timings; $\min p = 0.33$). However, we found the significant interaction between the age the EMG score of EBR induced by the auditory probe at 5.9 sec after the positive picture onset (1.9 sec post-stimulus offset). The results are displayed in Figure 8. The effect peaked on the dorsal part of the centromedial group of the right amygdala ($\max F = 16.71, p = 0.02$) [2], which is known as closely involved in such a startle reflex [8].

To illustrate the age interaction with the EMG scores more clearly, the population is divided into four age quantiles and the length is regressed over the standardized EMG scores covariating other variables at the vertex that gives the maximal F-statistic in Figure 8. Here we adjusted the length

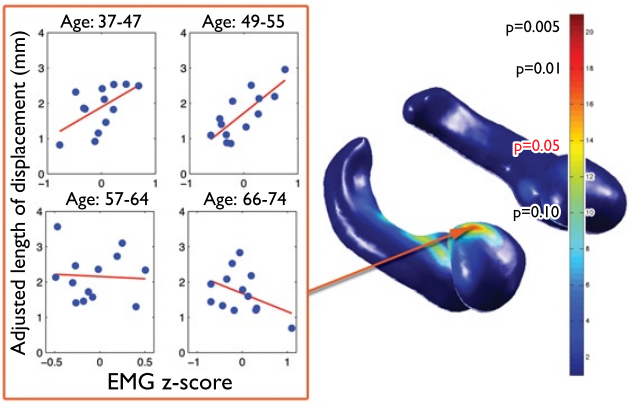

Figure 8: F-statistic maps showing the interaction between the ages and the standardized EMG scores. The regression plots are given at the vertex having the maximum F-statistic for each age quantile groups. Note that the interaction is illustrated by the different slopes of the regression lines.

by the lower degree model fit without the interaction term as

$$\begin{aligned} \mathrm{Residual} = \mathrm{Length} - (\widehat{\beta}_1 + \widehat{\beta}_2 \cdot \mathrm{Brain} + \widehat{\beta}_3 \cdot \mathrm{Age} \\ + \widehat{\beta}_4 \cdot \mathrm{Gender} + \widehat{\beta}_5 \cdot \mathrm{EMG}). \end{aligned} \tag{10}$$

The positive association between the emotional response and the anatomical feature of the right amygdala in the young population became negative in the old population. As the age effect in auditory startle reflex has been reported [14, 25], the interaction may reflect that the involvement of the central nucleus in startle pathway is altered as the age increases.

4. Conclusion

We have presented a new subcortical structure shape modeling framework based on the sparse representation of Fourier coefficients constructed with the LB-eigenfunctions. The proposed framework demonstrated higher sensitivity in modeling shape variations compared to the traditional volumetric analysis. The ability to localize subtle morphological difference may provide an anatomical evidence for the functional organization within human subcortical structures.

Acknowledgments

This research was supported by WCU program through the KOSEF funded by the MEST, Korea (R31-10089) to MKC and by grants from the National Institute of Aging

(P01-AG20166) to RJD. We also like to thank Seongho Seo of the Department of Brain and Cognitive Sciences, Seoul National University and Shubing Wang of Merck for the discussion on the sparse shape representation.

References

[1] R. Adler. On excursion sets, tube formulas and maxima of random fields. *Annals of Applied Probability*, pages 1–74, 2000.

[2] K. Amunts, O. Kedo, M. Kindler, P. Pieperhoff, H. Mohlberg, N. Shah, U. Habel, F. Schneider, and K. Zilles. Cytoarchitectonic mapping of the human amygdala, hippocampal region and entorhinal cortex: intersubject variability and probability maps. *Anatomy and Embryology*, 210(5):343–352, 2005.

[3] A. Andrade, F. Kherif, J. Mangin, K. Worsley, A. Paradis, O. Simon, S. Dehaene, D. Le Bihan, and J.-B. Poline. Detection of fmri activation using cortical surface mapping. *Human Brain Mapping*, 12:79–93, 2001.

[4] B. Avants, C. Epstein, M. Grossman, and J. Gee. Symmetric diffeomorphic image registration with cross-correlation: Evaluating automated labeling of elderly and neurodegenerative brain. *Medical Image Analysis*, 12(1):26–41, 2008.

[5] E. Bigler, D. Blatter, C. Anderson, S. Johnson, S. Gale, R. Hopkins, and B. Burnett. Hippocampal volume in normal aging and traumatic brain injury. *American Journal of Neuroradiology*, 18(1):11, 1997.

[6] M. Chung and J. Taylor. Diffusion smoothing on brain surface via finite element method. In *Biomedical Imaging: Nano to Macro, 2004. IEEE International Symposium on*, pages 432–435. IEEE, 2004.

[7] M. Chung, K. Worsley, B. Nacewicz, K. Dalton, and R. Davidson. General multivariate linear modeling of surface shapes using surfstat. *NeuroImage*, 53(2):491 – 505, 2010.

[8] M. Davis. Neural systems involved in fear and anxiety measured with fear-potentiated startle. *American Psychologist*, 61(8):741, 2006.

[9] A. Du, N. Schuff, L. Chao, J. Kornak, W. Jagust, J. Kramer, B. Reed, B. Miller, D. Norman, H. Chui, et al. Age effects on atrophy rates of entorhinal cortex and hippocampus. *Neurobiology of Aging*, 27(5):733–740, 2006.

[10] C. Good, I. Johnsrude, J. Ashburner, R. Henson, K. Friston, and R. Frackowiak. Cerebral asymmetry and the effects of sex and handedness on brain structure: a voxel-based morphometric analysis of 465 normal adult human brains. *NeuroImage*, 14(3):685–700, 2001.

[11] C. Good, I. Johnsrude, J. Ashburner, R. Henson, K. Friston, and R. Frackowiak. A voxel-based morphometric study of ageing in 465 normal adult human brains. *NeuroImage*, 14(1):21–36, 2001.

[12] R. Gur, F. Gunning-Dixon, W. Bilker, and R. Gur. Sex differences in temporo-limbic and frontal brain volumes of healthy adults. *Cerebral Cortex*, 12(9):998–1003, 2002.

[13] S. Kim, K. Koh, M. Lustig, S. Boyd, and D. Gorinevsky. An interior-point method for large-scale l1-regularized least squares. *Selected Topics in Signal Processing, IEEE Journal of*, 1(4):606–617, 2007.

[14] M. Kofler, J. Muller, L. Reggiani, and J. Valls-Solé. Influence of age on auditory startle responses in humans. *Neuroscience letters*, 307(2):65–68, 2001.

[15] P. Lang, M. Bradley, and B. Cuthbert. International affective picture system (iaps): Digitized photographs, instruction manual, and affective ratings (tech. rep. no. a-6). *Gainesville: University of Florida*, 2005.

[16] B. Lévy. Laplace-beltrami eigenfunctions towards an algorithm that understands geometry. In *Shape Modeling and Applications, 2006. SMI 2006. IEEE International Conference on*, pages 13–13. IEEE, 2006.

[17] W. Lorensen and H. Cline. Marching cubes: A high resolution 3D surface construction algorithm. *ACM Siggraph Computer Graphics*, 21(4):163–169, 1987.

[18] R. Malladi and I. Ravve. Fast difference schemes for edge enhancing Beltrami flow. In *Computer Vision – ECCV 2002*, volume 2350 of *Lecture Notes in Computer Science*, pages 343–357. Springer Berlin / Heidelberg, 2002.

[19] A. Miller, R. Alston, and J. Corsellis. Variation with age in the volumes of grey and white matter in the cerebral hemispheres of man: measurements with an image analyser. *Neuropathology and Applied Neurobiology*, 6(2):119–132, 1980.

[20] P. Perona and J. Malik. Scale-space and edge detection using anisotropic diffusion. *Pattern Analysis and Machine Intelligence, IEEE Transactions on*, 12(7):629–639, 1990.

[21] A. Qiu, D. Bitouk, and M. Miller. Smooth functional and structural maps on the neocortex via orthonormal bases of the laplace-beltrami operator. *Medical Imaging, IEEE Transactions on*, 25(10):1296–1306, 2006.

[22] A. Qiu and M. Miller. Multi-structure network shape analysis via normal surface momentum maps. *NeuroImage*, 42(4):1430–1438, 2008.

[23] N. Raz, U. Lindenberger, K. Rodrigue, K. Kennedy, D. Head, A. Williamson, C. Dahle, D. Gerstorf, and J. Acker. Regional brain changes in aging healthy adults: general trends, individual differences and modifiers. *Cerebral Cortex*, 15(11):1676, 2005.

[24] S. Seo, M. Chung, and H. Vorperian. Heat kernel smoothing using Laplace-Beltrami eigenfunctions. In *Medical Image Computing and Computer-Assisted Intervention – MICCAI 2010*, volume 6363 of *Lecture Notes in Computer Science*, pages 505–512. Springer, 2010.

[25] D. Smith, C. Hillman, and A. Duley. Influences of age on emotional reactivity during picture processing. *The Journals of Gerontology Series B: Psychological Sciences and Social Sciences*, 60(1):P49, 2005.

[26] S. Smith. Fast robust automated brain extraction. *Human Brain Mapping*, 17(3):143–155, 2002.

[27] N. Sochen, R. Kimmel, and R. Malladi. A general framework for low level vision. *Image Processing, IEEE Transactions on*, 7(3):310–318, 1998.

[28] M. Styner, I. Oguz, S. Xu, C. Brechbuhler, D. Pantazis, J. Levitt, M. Shenton, and G. Gerig. Framework for the statistical shape analysis of brain structures using spharm-pdm. In *Insight Journal, Special Edition on the Open Science Workshop at MICCAI*, 2006. http://hdl.handle.net/1926/215.

[29] E. Sullivan, L. Marsh, D. Mathalon, K. Lim, and A. Pfefferbaum. Age-related decline in mri volumes of temporal lobe gray matter but not hippocampus. *Neurobiology of Aging*, 16(4):591–606, 1995.

[30] E. Sullivan, L. Marsh, and A. Pfefferbaum. Preservation of hippocampal volume throughout adulthood in healthy men and women. *Neurobiology of aging*, 26(7):1093, 2005.

[31] B. Tang, G. Sapiro, and V. Caselles. Direction diffusion. In *The Proceedings of the Seventh IEEE International Conference on Computer Vision*, pages 2:1245–1252, 1999.

[32] G. Taubin. Geometric signal processing on polygonal meshes. In *Eurographics 2000 – State of the Art Report*, 2000.

[33] K. Walhovd, A. Fjell, I. Reinvang, A. Lundervold, A. Dale, D. Eilertsen, B. Quinn, D. Salat, N. Makris, and B. Fischl. Effects of age on volumes of cortex, white matter and subcortical structures. *Neurobiology of Aging*, 26(9):1261–1270, 2005.

[34] K. Walhovd, L. Westlye, I. Amlien, T. Espeseth, I. Reinvang, N. Raz, I. Agartz, D. Salat, D. Greve, B. Fischl, et al. Consistent neuroanatomical age-related volume differences across multiple samples. *Neurobiology of Aging*, 2009.

[35] K. Worsley, A. Evans, S. Marrett, and P. Neelin. A three-dimensional statistical analysis for CBF activation studies in human brain. *Journal of Cerebral Blood Flow and Metabolism*, 12:900–900, 1992.

[36] K. Worsley, S. Marrett, P. Neelin, A. Vandal, K. Friston, A. Evans, et al. A unified statistical approach for determining significant signals in images of cerebral activation. *Human brain mapping*, 4(1):58–73, 1996.

[37] Y. Xu, D. Valentino, A. Scher, I. Dinov, L. White, P. Thompson, L. Launer, and A. Toga. Age effects on hippocampal structural changes in old men: the haas. *NeuroImage*, 40(3):1003–1015, 2008.

[38] P. Yushkevich, B. Avants, J. Pluta, S. Das, D. Minkoff, D. Mechanic-Hamilton, S. Glynn, S. Pickup, W. Liu, J. Gee, et al. A high-resolution computational atlas of the human hippocampus from postmortem magnetic resonance imaging at 9.4 t. *Neuroimage*, 44(2):385–398, 2009.

[39] H. Zhang, O. van Kaick, and R. Dyer. Spectral methods for mesh processing and analysis. In *Eurographics 2007 – State of the Art Reports*, pages 1–22, 2007.